Inorganic Chemistry

Article

pubs.acs.org/IC

Vibrational Origin of the Thermal Stability in the Highly Distorted α-Quartz-Type Material GeO_2: An Experimental and Theoretical Study

Guillaume Fraysse,*[,†,§] Adrien Lignie,[†] Patrick Hermet,[†] Pascale Armand,*[,†] David Bourgogne,[†] Julien Haines,[†] Bertrand Ménaert,[‡] and Philippe Papet[†]

[†]Institut Charles Gerhardt Montpellier (ICGM), UMR 5253 CNRS-UM2-ENSCM-UM1, équipe C2M, Université Montpellier II, Place Eugène Bataillon, 34095 Montpellier cedex 5, France

[‡]Département Matière Condensée, Matériaux et Fonctions, Institut Néel, 25 avenue des Martyrs, Bâtiment F, BP 166, 38042 Grenoble cedex 9, France

ABSTRACT: We report an experimental and theoretical vibrational study of the high-performance piezoelectric GeO_2 material. Polarized and variable-temperature Raman spectroscopic measurements on high-quality, water-free, flux-grown α-quartz GeO_2 single crystals combined with state-of-the-art first-principles calculations allow the controversies on the mode symmetry assignment to be solved, the nature of the vibrations to be described in detail, and the origin of the high thermal stability of this material to be explained. The low-degree of dynamic disorder at high-temperature, which makes α-GeO_2 one of the most promising piezoelectric materials for extreme temperature applications, is found to originate from the absence of a libration mode of the GeO_4 tetrahedra.

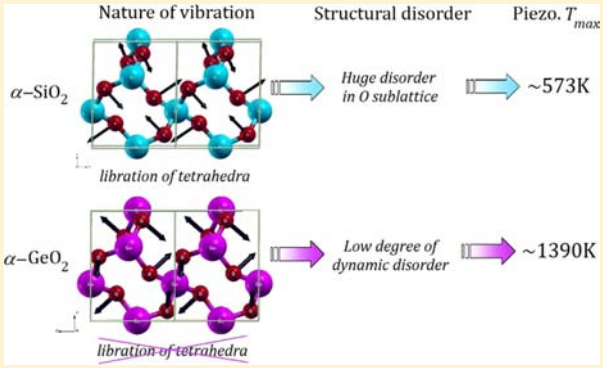

1. INTRODUCTION

Recently, there has been a growing demand for smart transducers and sensors that can function at extreme temperatures and harsh environments without failure. Due to numerous advantages over other sensing approaches, such as fast response time, ease of integration, simple structures, good thermal stability and sensitivity, piezoelectric-based sensors have generated great interest among aerospace, aircraft, automotive, and nuclear industries.[1] Nevertheless, new piezoelectric materials that can function at extreme temperatures are required for the next generation of high-temperature sensors (the operational temperature range being limited by the sensing capability of the piezoelectric material at elevated temperatures, increased conductivity and mechanical attenuation, variation of the piezoelectric properties with temperature, phase transitions).[1−3] Current research on materials for high-temperature applications focuses essentially on three classes of piezoelectric crystals, namely, quartz analogues ABO_4,[4−7] langasite-type compounds $A_3BC_3D_2O_{14}$,[8] and oxyborate crystals $ReCa_4O(BO_3)_3$.[9] Among quartz analogues, α-quartz germanium dioxide (GeO_2) and gallium arsenate ($GaAsO_4$) exhibit the highest thermal stability and the highest electromechanical coupling coefficient k.[10,11] If at first more attention was paid to the former owing to the close chemical analogy of GeO_2 to SiO_2 and concerns regarding the toxicity of arsenic, the crystal growth of large α-quartz GeO_2 single crystals has been for a long time an intractable challenge. Difficulties originated from the "metastability" of the α-quartz phase with respect to the rutile form and the presence of hydroxyl groups in the crystals catalyzing the transition to the thermodynamically stable rutile structure. The recent development of the slow-cooling method in selected inorganic fluxes, an original technique which in contrast to the conventional hydrothermal technique does not require aqueous media, proved to be a breakthrough in the growth of large high-quality water-free single crystals.[12,13] α-Quartz GeO_2 is now expected to be one of the most promising materials for extreme temperature applications. This highly distorted (θ = 130.0°, δ = 26.6°) α-quartz homeotype is characterized by an electromechanical coupling coefficient k that is more than twice that of α-quartz.[14] Furthermore, it does not exhibit phase transitions before melting (in the α-quartz family the thermal stability of the tetrahedral tilt angle δ, which is the order parameter for the $\alpha \leftrightarrow \beta$ phase transition, strongly depends on the initial degree of structural distortion).[11] Thus, contrary to what has been found for other α-quartz materials, except for α-$GaAsO_4$,[4,15] no discontinuity in the piezoelectric properties is expected.

Now, it should be noted that the existence of an α-quartz to β-quartz (e.g., in α-quartz, α-$AlPO_4$, α-$FePO_4$) or β-cristobalite (in α-$GaPO_4$) phase transition restricts the temperature range for applications to well below the critical temperature.

Received: April 16, 2013
Published: June 4, 2013

   dx.doi.org/10.1021/ic4009416 | *Inorg. Chem.* 2013, 52, 7271−7279

Piezoelectric measurements coupled with total neutron scattering measurements have shown indeed a degradation of the mechanical quality factor Q of the resonators (a measure of the quality of the resonator with respect to acoustic attenuation), linked to increasing structural disorder that begins 200−300 K below the phase transition temperature [α-quartz (respectively α-$GaPO_4$) retaining its piezoelectric properties up to ∼573 K (respectively ∼1023 K) instead of 846 K (respectively 1206 K)].[16,17] In this temperature range, the onset of considerable disorder in the oxygen sublattice is observed, which rapidly dissipates the induced dipoles, resulting in the observed decrease of the mechanical quality factor Q. Thus, because of the absence of any phase transition, the degree of thermally induced dynamic disorder in α-quartz GeO_2 could be expected to be low up to its melting point. However, no investigation on dynamic disorder has been performed up to now. On the basis of the variation in wavenumber and line width, Raman spectroscopy can give relevant information regarding the anharmonicity of vibrations.[18]

In the present study, we thus report polarized and variable-temperature Raman spectroscopic measurements performed on flux-grown α-quartz GeO_2 single crystals along with state-of-the-art density functional theory (DFT) based calculations. The wavenumbers of the Raman lines as well as their intensities for both the transverse optical (TO) and longitudinal optical (LO) modes have been determined. The excellent agreement obtained between experimental and theoretical Raman lines for both wavenumbers and relative intensities allows us to unambiguously assign the symmetry and the nature of α-quartz GeO_2 modes, clarifying the long-standing debate reported in the literature. In addition, vibrations in α-GeO_2 are shown to be very slightly anharmonic, as evidenced by the very low wavenumber shifts and the weak damping of the modes between room temperature and 1373 K. Furthermore, in contrast with what has been observed in other α-quartz homeotypes like SiO_2 or $AlPO_4$, which undergo an α-quartz to β-quartz phase transition, first-principles calculations reveal the absence of a tetrahedral libration mode. This explains the very low degree of thermally induced dynamic disorder present in flux-grown single crystals and further confirms that the piezoelectric properties of α-GeO_2 should not degrade significantly up to the melting point.

2. EXPERIMENTAL AND COMPUTATION DETAILS

High-quality, water-free, α-quartz-type GeO_2 single crystals grown by the flux method were investigated by polarized and variable-temperature Raman spectroscopy. Detailed information regarding the crystal growth, X-ray diffraction (XRD), energy dispersive X-ray (EDX), and Fourier transform infrared (FT-IR) spectroscopic analyses can be found elsewhere.[12,19]

Polarized Raman spectroscopy measurements were performed on a Jobin-Yvon T64000 spectrometer equipped with a single monochromator, an Olympus microscope, and a CCD cooled by nitrogen down to 140 K. The 488 nm line of an argon ion laser was used for excitation. As-grown single crystals were placed under the objective (50×) of the microscope and manually oriented in the appropriate direction. The laser power on the samples was typically 20 mW. A half-wave retardation plate was inserted before the microscope objective to rotate the polarization of the incident laser beam and of the scattered light. All Raman spectra were collected in backscattering configuration, with the incident and scattered light propagating perpendicular to the Y (010) or Z (001) face (in the orthogonal system) of GeO_2 single crystals. The orientation of crystals with reference to the polarization of the laser in both the incident and scattering directions is given in the conventional Porto notation [i.e., a four letters code expressing the incident direction (incident polarization, scattered polarization) scattering direction, e.g., $y(zz)\bar{y}$].[20]

Nonpolarized Raman spectra were obtained using the 473 nm excitation line of a blue diode laser with a Horiba Jobin-Yvon LabRam Aramis spectrometer equipped with an Olympus microscope and a CCD cooled by a thermoelectric Peltier device. Variable-temperature measurements were performed up to 1373 K on a single crystal of α-GeO_2 placed on a thin platinum block in the oven of a Linkam TS1500 heating stage under the 50× long focal length objective of the microscope. The temperature was measured by a thermocouple at the bottom of the oven. A 20 K/min heating rate was used to arrive at the desired temperatures. Spectra were collected in the 50−1200 cm^{-1} range after a 300 s period for temperature stabilization. The acquisition time was 20 s per spectrum irrespective of the temperature. The temperature uncertainty was estimated to be 30 K in the 473−873 K and 50 K in the 873−1373 K temperature ranges.

In both experiments, wavenumber stability and instrumental accuracy (on the order of ±0.5 cm^{-1}) were calibrated by recording the F_{2g} Raman-active mode of silicon at 521 cm^{-1}. After subtracting a linear background (or a second-order polynomial background in the case of variable-temperature measurements) positions, integrated intensities and full widths at half-maximum (fwhm) of Raman modes were obtained by fitting pseudo-Voigt functions to the data. The Raman signal of a commercial GeO_2 powder (PPM Pure Metals 99.999%) was also collected for comparison.

Dynamical matrix (yielding the phonon frequencies and eigenvectors) of α-quartz-type GeO_2 was calculated within the density functional perturbation theory framework as implemented in the ABINIT package.[21] Lattice parameters and atomic positions were relaxed. Calculations were performed within the local density approximation using Perdew−Wang parametrization.[22] Convergence was reached for a 70 Ha plane-wave kinetic energy cutoff and a 8 × 8 × 8 mesh of special k points. Raman intensities were obtained as described in ref 23.

3. RESULTS AND DISCUSSION

3.1. Analysis of the Raman Spectra. The Raman signal of a flux-grown α-quartz GeO_2 single crystal was first collected in the 50−4000 cm^{-1} range, and no other mode than the four nondegenerate A_1 and the eight doubly degenerate E modes predicted by group theory for α-quartz-type GeO_2 (D_3 point group) was observed (Figure 1). In particular, no evidence of Raman bands that could be assigned to the rutile form of GeO_2 was found (the strongest A_{1g} mode arising from Ge−O stretching motions within octahedral GeO_6 groups should appear at 700 cm^{-1}).[24] Furthermore, whereas the Raman spectrum of the commercial GeO_2 powder exhibited an additional feature around 780 cm^{-1}, no band was detected in this frequency range for the flux-grown single crystal. This band, which is found to disappear once the commercial powder is annealed, has already been reported and assigned to oxygen vacancy complexes,[25] a Ge−OH vibration,[26] or a Ge−O stretching vibration of a water-distorted GeO_4 entity.[24,27] The absence of a Raman band centered around 3600 cm^{-1} should also be noted. Neither hydroxyl groups nor water inclusions are thus present in the as-grown α-GeO_2 crystal, in agreement with previous infrared measurements.[13] The nonpolarized Raman spectrum presented in Figure 1 is the signature of high-quality, water-free, flux-grown single crystals, which can be used to accurately determine the wavenumbers, symmetries, and damping of Raman modes.

Surprisingly, in spite of the relative simplicity of the trigonal α-quartz GeO_2 structure and the numerous experimental and theoretical Raman studies reported in the literature, there still remain a lot of contradictions and ambiguities about the mode

dx.doi.org/10.1021/ic4009416 | Inorg. Chem. 2013, 52, 7271−7279

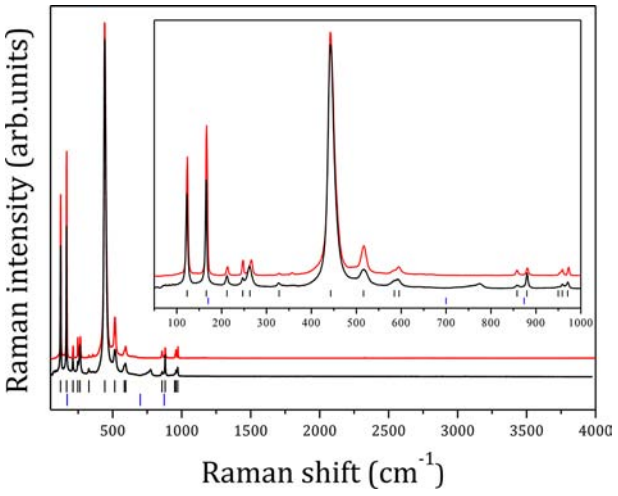

Figure 1. Nonpolarized room-temperature Raman spectra of a flux-grown single crystal (in red) and a commercial powder (in black) of α-quartz GeO_2. Vertical ticks indicate from the top down the positions of Raman modes in the α-quartz and rutile phases of GeO_2 as reported by Ranieri et al. and Kaindl et al.[36,24]

symmetries in particular at low frequency. Assignment of the Raman lines of α-quartz-type GeO_2 was reported for the first time by Scott in 1970[28] and then slightly revised by him in a subsequent study.[29] Despite important errors, these results were for a long time considered to be reliable, although the identification of the E lines was based exclusively on analogies with α-quartz. In the late 1980s, a significant improvement in the Raman mode assignments was reported by Avakyants et al.;[30] however, this work went largely unnoticed and many experimental and theoretical Raman spectroscopy studies continued to use the mode assignments of Scott and co-workers.[31−36]

In order to clarify this long-standing debate, polarized Raman spectroscopy measurements were performed on high-quality, water-free α-quartz GeO_2 single crystals, and the results were compared with state-of-the-art first-principles calculations. The Raman signal was first collected in backscattering configuration with the incident and scattered light propagating perpendicular to the *Y* face of the crystal (Figure 2) and with the incident and scattered polarization along the *z*-axis so that all the modes should disappear except those of A_1 symmetry. The resulting along with the calculated spectra are shown in Figure 3a. Excellent agreement between experimental and calculated

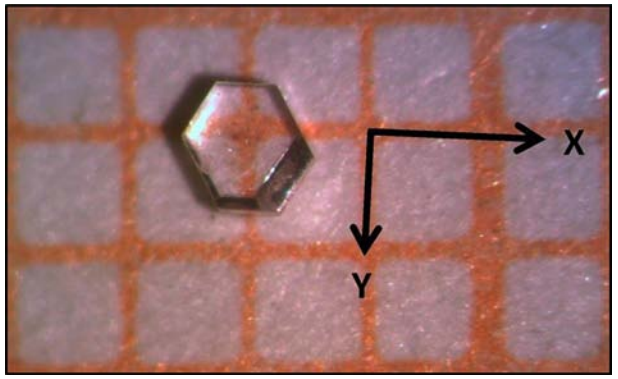

Figure 2. Photograph of the *Z* (001) face (in the orthogonal system) of an α-quartz GeO_2 single crystal on a millimetric grid.

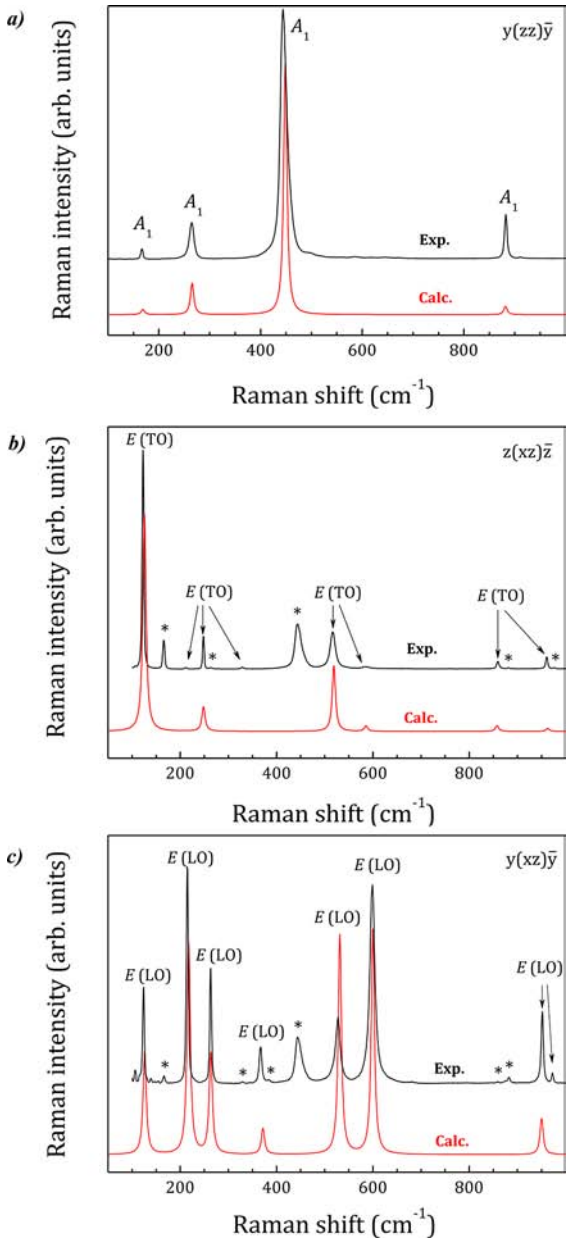

Figure 3. Calculated and experimental Raman spectra of α-GeO_2 for three scattering configurations with the incident and scattered light propagating perpendicular to the (a, c) *Y* face or (b) *Z* face of the crystal and with the incident (respectively scattered) polarization along the (a) *z*-axis (respectively *z*-axis) or (b, c) *x*-axis (respectively *z*-axis). Star symbols in the experimental spectra indicate the positions of α-GeO_2 modes, which have not totally disappeared due to a slight deviation from the ideal orientation.

spectra is found for both positions and relative intensities. This allows us to unambiguously assign the four experimental Raman lines located at room temperature at 166, 264, 445, 882 cm^{-1} to A_1 symmetry modes. This result is already in disagreement with what has been reported in the literature as the mode observed around 166 cm^{-1} has been almost always assigned to a double-degenerate E mode.[28,29,31,32,34,36] Only Avakyants et al. and Kaindl et al. have reported A_1 symmetry for this mode.[30,24] Similarly, if the mode located around 212 cm^{-1} was correctly assigned by Scott in his second paper,[29] some authors still have used his first assignment and have thus assigned this mode as A_1.[31,32]

dx.doi.org/10.1021/ic4009416 | Inorg. Chem. 2013, 52, 7271−7279

Table 1. Experimental Raman Wavenumbers of a Flux-Grown α-Quartz GeO_2 Single Crystal at 293 K and Calculated Values at 0 K[a]

symmetry	calcd (cm^{-1})	expl (cm^{-1})	Δ (cm^{-1})	fwhm (cm^{-1})	proposed assignment[b]	S_{tot} (S^{Ge})[c]
E (TO1)	126	123	3	4	τ O−Ge−O	0.78 (0.12)
E (LO1)	126	124	2	4	τ O−Ge−O	0.86 (0.12)
A_1 (TO1)	169	166	3	5	τ Ge−O−Ge + ρ O−Ge−O	0.59 (0.43)
E (TO2)	214	212	2	4	τ O−Ge−O + τ Ge−O−Ge	0.81 (0.27)
E (LO2)	217	215	2	5	τ O−Ge−O + τ Ge−O−Ge	0.75 (0.26)
E (TO3)	248	248	0	4	τ O−Ge−O + τ Ge−O−Ge	0.77 (0.43)
E (LO3)	263	263	0	4	τ Ge−O−Ge + ω O−Ge−O	0.83 (0.47)
A_1 (TO2)	265	264	1	10	τ O−Ge−O	0.82 (0.01)
E (TO4)	332	329	3	7	τ O−Ge−O + τ Ge−O−Ge	0.89 (0.30)
E (LO4)	372	367	5	6	τ Ge−O−Ge + δ O−Ge−O	0.81 (0.25)
A_1 (TO3)	449	445	4	16	τ O−Ge−O	0.83 (0.03)
E (TO5)	519	517	2	13	ρ O−Ge−O + τ Ge−O−Ge	0.84 (0.28)
E (LO5)	531	527	4	12	τ O−Ge−O + τ Ge−O−Ge	0.88 (0.29)
E (TO6)	586	586	0	13	δ O−Ge−O + τ Ge−O−Ge	0.85 (0.28)
E (LO6)	600	599	1	12	ω O−Ge−O + τ Ge−O−Ge	0.79 (0.25)
E (TO7)	858	859	−1	6	ρ O−Ge−O	0.80 (0.12)
A_1 (TO4)	882	882	0	6	τ O−Ge−O	0.88 (0.11)
E (LO7)	950	952	−2	5	ρ O−Ge−O + ν_s O−Ge−O	0.78 (0.11)
E (TO8)	963	961	2	5	ν_s O−Ge−O	0.78 (0.06)
E (LO8)	976	973	3	4	ν_s O−Ge−O	0.82 (0.12)

[a]Deviation (Δ) between calculated and experimental wavenumbers, full widths at half-maximum (fwhm), mode assignments, and localization entropy of modes are also reported. [b]τ, twisting; ω; wagging; δ; scissoring; ρ; rocking; ν_s, symmetric stretching. Twisting and wagging are out-of-plane bending, whereas scissoring and rocking are in-plane bending. [c]S_{tot} is the total localization entropy according to eq 1, whereas S^{Ge} is the localization entropy on Ge atoms (in parentheses).

The $z(xz)\bar{z}$ polarization configuration was then used to activate only the transverse optical E modes. Even if some A_1 and E (LO) modes did not totally disappear due to a slight deviation from the ideal orientation, the expected eight modes are observed at a wavenumber position very close to the calculated ones (Figure 3b). Their relative intensities are also found to be in excellent agreement with the calculation. The modes centered at 123, 212, 248, 329, 517, 586, 859, and 961 cm^{-1} in the room-temperature experimental spectrum can be thus unambiguously assigned to E (TO) modes. Once again, important discrepancies between our results and those reported in previous studies are found. For instance, while the mode located around 517 cm^{-1} has been always assigned to a longitudinal mode (even in the very recent study reported by Kaindl et al.),[24] this mode is shown to be actually a transverse E (TO) mode. Furthermore, if the line around 329 cm^{-1} was correctly assigned to an E (TO) mode in the first report of Scott, the author subsequently revised his assignment to A_1 symmetry. Studies that were based on the second assignment have thus propagated this error.[34,36] Some Raman lines have also been reported at 385 and 456 cm^{-1} and have been assigned by Scott, Dultz et al., Gillet et al., and Micoulaut et al. to a E (TO) and E (LO) doublet, while they in fact do not arise from vibrations of α-GeO_2.[28,29,31,34] This incorrect assignment can be explained by the fact that there is actually a double-degenerate E mode at lower frequency [close to the A_1 (TO2) mode], which could not have been detected at that time. Furthermore, even if Avakyants et al. succeeded in detecting the E lines around 260 cm^{-1} the E (TO) mode was incorrectly located at a higher frequency than the A_1 (TO2) mode.[30] Kaindl et al. have also assigned the mode at ~960 cm^{-1} to a longitudinal E (LO), whereas it is actually a transverse mode.[24]

Finally, the eight longitudinal E (LO) modes are obtained with the incident and scattered light propagating perpendicular to the *Y* face of a GeO_2 single crystal and with the incident and scattered polarization along the *x*- and *z*-axis respectively (Figure 3c). The low-intensity modes located at 124, 215, 263, 367, 527, 599, 952, and 973 cm^{-1} can in turn be definitively assigned to E (LO) modes. It should be noted that the spectrometer configuration favors the A_1 mode over the others and thus that it is not easy to make the former totally disappear. As found for A_1 and E (TO) modes, the present results are significantly different from what has been reported in the literature. For instance, Kaindl et al. have assigned the modes located around 936 and 952 cm^{-1} to E (LO) and E (TO) modes, respectively, although the former does not correspond to a structural vibration of α-GeO_2 and the latter is actually the longitudinal E (LO7) mode.[24]

The wavenumbers of the four nondegenerate A_1 and the eight doubly degenerate E modes observed at room temperature are reported in Table 1 along with the calculated values. Full widths at half-maximum determined from experimental Raman spectra are also given. The excellent agreement obtained between experimental and theoretical Raman lines for both positions and relative intensities indicates that (i) our computational methodology based on the nonlinear response formalism and the $2n + 1$ theorem appears to efficiently describe the change of optical dielectric susceptibility induced by individual atomic displacements (quantity required to compute the intensity of the Raman modes)[23] in the α-quartz type structure, (ii) flux-grown single crystals of α-quartz GeO_2 are of high chemical quality, and (iii) vibrations in the α-quartz GeO_2 structure are relatively quasiharmonic, as the calculated frequencies—at 0 K—are almost the same as the experimental values—at 298 K. This issue will be discussed in section 3.3.

3.2. Assignment of the Raman Lines. As for the symmetry of the α-GeO_2 Raman lines, some contradictions and ambiguities still remain in the literature on their assignment

dx.doi.org/10.1021/ic4009416 | Inorg. Chem. 2013, 52, 7271−7279

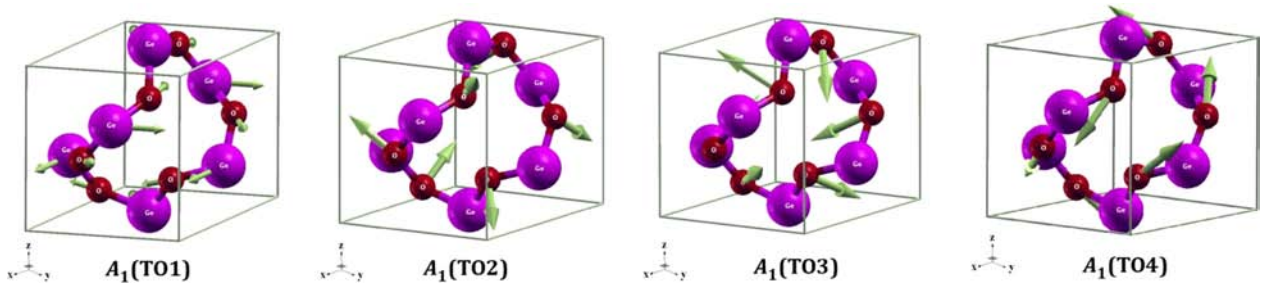

Figure 4. Calculated vibrational modes of α-quartz GeO_2 at 169 cm^{-1} [A_1 (TO1)], 265 cm^{-1} [A_1 (TO2)], 449 cm^{-1} [A_1 (TO3)], and 882 cm^{-1} [A_1 (TO4)]. Large purple and small red spheres represent Ge and O atoms, respectively. Eigenvectors (in green) are plotted with a different scale for the four A_1 modes. Arrows are proportional to the amplitude of the atomic displacements.

to specific atomic motions. For instance, four different frequency ranges could be distinguished according to Parke et al.:[37] (i) Raman lines up to 300 cm^{-1} may be complex translations and rotations of the GeO_4 tetrahedra, (ii) those in the 300−350 cm^{-1} range could be Ge−O bending vibrations, (iii) the majority of the lines in the midfrequency region up to 590 cm^{-1} are assigned to Ge−Ge stretching motions, and (iv) the Ge−O stretching motions within tetrahedral GeO_4 units are believed to be responsible of Raman lines in the high-frequency region.[37] In contrast, only two different frequency ranges have been reported in the recent experimental and theoretical Raman spectroscopy study of Kaindl et al.:[24] the first range ending at ∼590 cm^{-1} is assigned to O−Ge−O or Ge−O−Ge bending vibrations, while the second range (840−970 cm^{-1}) could be dominated by Ge−O−Ge and O−Ge stretching vibrations.[24] Similarly, the main A_1 (TO3) line is not unambiguously assigned. Indeed, Mernargh et al. have assigned this line to symmetrical Ge−O−Ge stretching,[32] while according to Ranieri et al. it rather corresponds to a O−Ge−O bending vibration.[36] Furthermore, first-principles calculations of Raman frequencies recently performed by Kaindl et al. have assigned this line to Ge−O−Ge bending.[24]

To clarify this long-standing debate, we analyzed the eigendisplacement vectors of each normal mode obtained from the diagonalization of the dynamical matrix. In contrast with the work from Kaindl et al., who have assigned the Raman lines on the basis of the comparison between the experimental and calculated frequencies without consideration of their intensities,[24] we included their intensities in our calculations. The close agreement observed in Figure 3 between theory and experiment therefore allows convincing mode assignments. To improve the accuracy of our assignments, we also computed the localization entropy defined as

$$S_j = -\frac{1}{\ln(3N)} \sum_{\delta,n} |\langle n\delta|j\rangle|^2 \ln(|\langle n\delta|j\rangle|^2) \quad (1)$$

where the sum runs over all atoms n and space directions δ, $\langle n\delta|j\rangle$ is the $(n\delta)$-component of the jth phonon eigenvector, and N is the total number of atoms inside the unit cell. The above-defined localization entropy is connected with the lack of information about the position of the jth phonon mode and gives the same kind of information as the participation ratio. If the mode is perfectly localized, then the lack of information is minimal, and only one of the $|\langle n\delta|j\rangle|^2$ is equal to 1, which leads to $S_j = 0$. On the other hand, if the jth mode is completely delocalized, then $|\langle n\delta|j\rangle|^2 = 1/3N$, $\forall n\delta$, and S_j is the maximum, i.e., equal to 1. Here, S_j has been normalized to 1 for convenience; thus, it is not a genuine entropy. Now, let us consider the case where the jth mode is fully localized on Ge atoms. The value of S_j would then be around $S_j^{Ge} = \ln(3N_{Ge})/\ln(3N)$, where N_{Ge} is the number of Ge atoms in the unit cell. Thus, if a mode is localized on Ge atoms, the corresponding S_j^{Ge} would be close to $\ln(3 \times 3)/\ln(3 \times 9) = 2/3$.

Our assignments of the Raman lines based on the analysis of their eigendisplacement vectors and their localization entropies are reported in Table 1. From this table, it is clear that the Raman modes do not correspond to very localized modes, since their localization entropies lie around 0.82 and are never smaller than 0.75, except for the A_1 (TO1) mode. The latter is almost localized on Ge atoms, as its localization entropy on Ge atoms is 0.43 (0.67 if fully localized on Ge atoms). Raman lines in α-quartz GeO_2 are therefore assigned to complex atomic motions of tetrahedra, and no clear limit between pure intratetrahedral vibrations and mixed inter/intratetrahedral vibrations can be unambiguously observed (see Table 1). However, motions of Ge atoms mainly dominate the E modes between 200 and 600 cm^{-1}, as their localization entropies are above 0.25, whereas O atoms are mainly involved on the A_1 modes in this frequency range. The atomic motions on the Ge and O atoms have similar magnitudes for the E (TO3) and E (LO3) modes, only. They are assigned to a combination of out-of-plane bending of tetrahedra. In contrast to Kaindl et al.,[24] who have assigned the 845−975 cm^{-1} range to Ge−O−Ge or O−Ge stretching modes, we assign the modes between 845 and 950 cm^{-1} to O−Ge−O out-of-plane bending and the remaining modes up to 975 cm^{-1} to O−Ge−O stretching. The eigendisplacement vectors of the four A_1 modes are displayed in Figure 4. The A_1 (TO1) line at 166 cm^{-1} is a combination mode involving O−Ge−O rocking and Ge−O−Ge twisting, whereas the A_1 (TO2) line at 264 cm^{-1} is dominated by O−Ge−O twisting. These two modes will be relevant to understand the origin of the high thermal stability of α-quartz GeO_2 (see section 3.3). Contrary to what was reported by Mernagh et al.,[32] Parke et al.,[37] and Kaindl et al.,[24] we assign the A_1 (TO3) line as O−Ge−O twisting. This assignment is supported by the weak localization factor on Ge atoms (0.03).

3.3. Origin of the High-Thermal Stability. As-collected variable-temperature Raman spectra of α-GeO_2 are reported in Figure 5. No drastic change can be seen with increasing temperature. Even at the highest temperature reached, i.e., 1373 K, the Raman signal still exhibits the features of an α-quartz-type structure, confirming thus, at a local level, the high-thermal stability of the material previously observed by differential scanning calorimetry and X-ray and neutron diffraction measurements.[11,13] The lack of any additional lines in particular around 700 cm^{-1} clearly demonstrates the absence of a temperature-induced α-quartz to rutile phase transition, in

dx.doi.org/10.1021/ic4009416 | Inorg. Chem. 2013, 52, 7271−7279

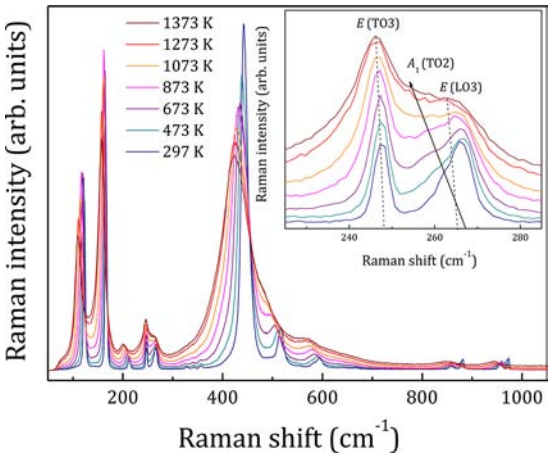

Figure 5. As-collected Raman signal of α-quartz GeO_2 as a function of increasing temperature (the plot of as-collected spectra allows the evolution in wavenumber and line width to be seen at a glance). The inset illustrates the temperature dependence of A_1 (TO2), E (TO3), and E (LO3) modes near 260 cm^{-1}.

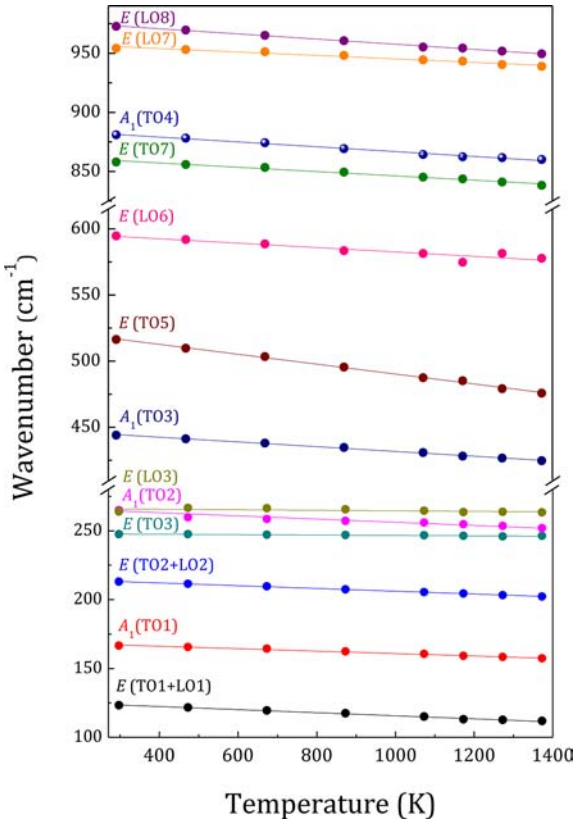

Figure 6. Temperature shifts of Raman modes. Wavenumber uncertainties are smaller than the symbol size. Results of the linear fit are also plotted.

contrast to what has been previously reported by Gillet et al. and Bielz and co-workers.[31,27] The occurrence of any $\alpha \leftrightarrow \beta$ phase transition can also be ruled out, as the most intense A_1 line is found to shift and broaden in a continuous linear way (Ranieri et al. have shown that this transition can be evidenced not only by the presence of soft modes, but also by an abrupt change in the evolution of both the wavenumber shift and line width of the O−(Si/Ge)−O intratetrahedra bending vibrational mode).[36]

Additionally, the wavenumber of the different Raman modes is found to decrease with increasing temperature due to the softening of the effective force constants (Figure 6). The shifts are however relatively small. This is particularly obvious for the E (TO3) and E (LO3) modes, which hardly soften with increasing temperature (their positions shift by less than 2 cm^{-1} in the whole temperature range investigated). It should be noted that the shift of the E (TO5) mode is widely overestimated. During the curve fitting, this mode actually counterbalances the asymmetric shape of the main band. Temperature shifts of Raman modes are added in Table II along with those reported in previous studies.[31,32] Overall similar values of $(\delta\nu_i/\delta T)_P$ are obtained, but one discrepancy should be noted. Due to the incorrect assignment of the E (TO3) and E (LO3) modes, which are in fact located close to a second A_1 (TO2) mode, Gillet et al. have overestimated the temperature shift of the latter (−0.015 cm^{-1} K^{-1} instead of −0.011 cm^{-1} K^{-1}).[31] This is not insignificant, as this A_1 symmetry mode involving only oxygen displacements is the mode corresponding to the libration mode of the tetrahedra in α-SiO_2. Contrary to what has been found in α-quartz and α-berlinite, which undergo an $\alpha \leftrightarrow \beta$ phase transition, this mode does not soften in α-GeO_2.

Similarly, small increases in the line width are found for almost all the modes. What could be considered incorrectly as a significant increase in the line width of the E (TO3) and E (LO3) modes is actually due to a stronger shift of the neighboring A_1 (TO2) mode lying in between them (see the inset of Figure 5). At 1373 K, the latter as well as most of Raman modes have broadened by less than 11 cm^{-1} with respect to their room temperature values (Figure 7). As for the shift in position, the high value of the E (TO5) mode fwhm cannot be considered as reliable, as this band tends to merge with the main line at high temperature. Furthermore, distinguishing the low-intensity, high-frequency modes from the background contribution becomes more and more difficult with increasing temperature. Thus, the fwhm of high-frequency modes are probably overestimated too. Even close to the melting temperature, only the full width at half-maximum of the A_1 (TO3) mode has increased significantly.

Thus, except for the main A_1 (TO3) mode centered at 445 cm^{-1} at room temperature and the neighboring E (TO5) mode, variations in line width as well as in wavenumbers are relatively small between 298 and 1373 K. These results indicate that anharmonicity does not increase significantly with increasing temperature. The weak damping of the A_1 (TO2) suggests also that flux-grown α-quartz GeO_2 single crystals are characterized by a very low degree of thermally induced dynamic disorder, even close to the melting point. This issue is of prime importance for high-temperature applications, as the thermally induced dynamic disorder found in other α-quartz materials well below their $\alpha \leftrightarrow \beta$ phase transition temperature has been shown to induce a loss of correlation between dipoles, resulting in a decrease of the mechanical quality factor Q. In order to understand the origin of the low degree of thermally induced dynamic disorder in α-GeO_2, it should be noted that the significant dynamic disorder present in α-quartz and berlinite has been shown to arise from the thermally excited rigid unit modes (RUM) corresponding to the libration of the constituent essentially rigid tetrahedra.[16,38,39] This tetrahedral A_1 libration mode softens and broadens significantly upon increasing temperature. Now, in contrast to α-SiO_2 and α-

dx.doi.org/10.1021/ic4009416 | Inorg. Chem. 2013, 52, 7271−7279

Table II. Temperature Shifts $\delta\nu_i/\delta T$ (cm^{-1} K^{-1}) of Raman Modes Compared to Those Reported by Gillet et al. and Mernagh et al.[31,32] [a]

		$\delta\nu_i/\delta T$ (cm^{-1} K^{-1})		
wavenumber (cm^{-1})		present study	Gillet et al.[31]	Mernagh et al.[32]
T = 293 K	mode symmetry	293−1373 K	293−1273 K	109−874 K
123	E (TO1 + LO1)	−0.011(1)	−0.009(1)	−0.009
166	A_1 (TO1)	−0.009(1)	−0.008(1)	−0.006
212	E (TO2 + LO2)	−0.010(1)	−0.011(1)	−0.008
248	E (TO3)	−0.001(1)		0.002
263	E (LO3)	−0.002(1)		−0.005
264	A_1 (TO2)	−0.011(2)	−0.015(3)	−0.007
329	*E* (TO4)	−0.005(1)*	+0.005(2)	
367	E (LO4)	−0.001(1)*		
445	A_1 (TO3)	−0.018(1)	−0.019(2)	−0.023
517	E (TO5)	−0.038(1)	−0.042(5)	−0.023
527	E (LO5)			
586	E (TO6)	−0.015(9)*	−0.022(3)	−0.021
599	E (LO6)	−0.017(3)	−0.022(3)	−0.016
859	E (TO7)	−0.018(1)	−0.015(2)	−0.010
882	A_1 (TO4)	−0.021(1)	−0.025	−0.023
952	E (LO7)	−0.015(1)		−0.014
961	E (TO8)	−0.016(4)*	−0.025(3)	−0.010
973	E (LO8)	−0.022(1)	−0.023(3)	−0.019

[a] Temperature ranges are noted. Asterisks indicate Raman modes that have been followed only from 293 to 673 K.

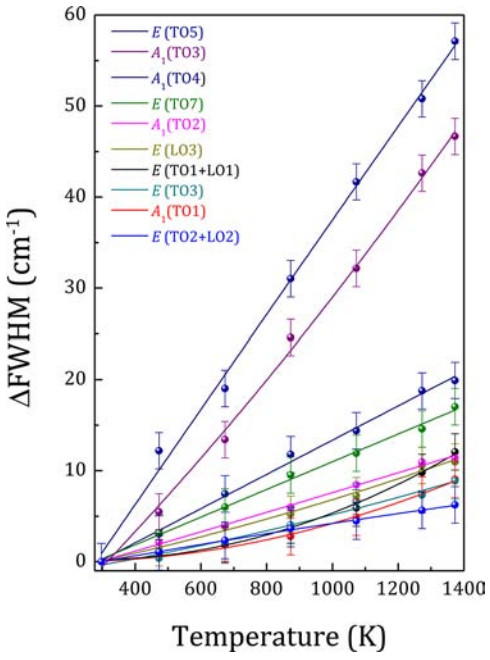

Figure 7. Relative full width at half-maximum (Δfwhm) of some selected α-GeO_2 Raman modes as a function of temperature (with respect to the room temperature value).

$AlPO_4$, the increase of damping on heating for the A_1 mode involving only oxygen displacements is very small in α-GeO_2. Furthermore, while the libration of the SiO_4 tetrahedra in SiO_2 corresponds to a tilting of the tetrahedra around the x axis and a rotation of O atoms in the (y, z) plane with identical components,[40] the corresponding mode in α-GeO_2 consists of O−Ge−O twisting (see Figure 8). This mode is thus definitively not a libration. The absence of tetrahedral libration mode and consequently instability has already been observed by Cambon et al. for the α-quartz-type gallium arsenate

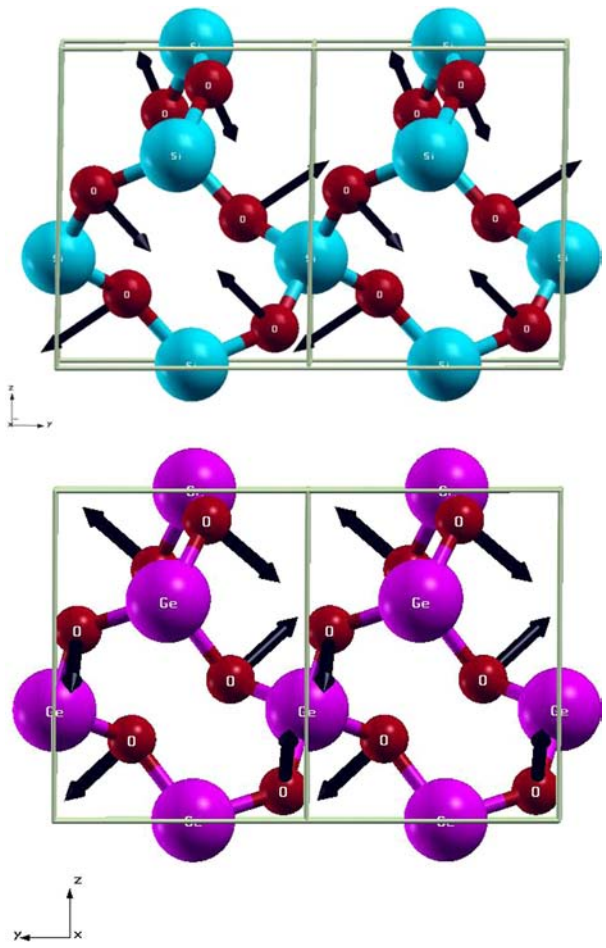

Figure 8. Eigenvectors of the A_1 mode at 218 cm^{-1} in α-quartz SiO_2 (top) and at 265 cm^{-1} in α-quartz GeO_2 (bottom).

dx.doi.org/10.1021/ic4009416 | Inorg. Chem. 2013, 52, 7271−7279

$GaAsO_4$.[41] This highly distorted material does not undergo a phase transition but decomposes at 1303 K.[6]

The low degree of thermally induced dynamic disorder reported here, along with the high thermal stability of the structure and the high crystalline quality that can be obtained by the slow cooling method, make flux-grown α-GeO_2 one of the most promising piezoelectric materials for high-temperature applications. Nevertheless, further high-temperature studies by total neutron scattering and piezoelectric measurements are encouraged in order to confirm the very low degree of thermally induced dynamic disorder present in these flux-grown α-quartz GeO_2 single crystals, as well as the expected low mechanical attenuation and the small variation of the piezoelectric properties at high temperature.

4. CONCLUSION

First-principles calculations coupled with polarized Raman spectroscopy measurements on high-quality, water-free, flux-grown α-quartz GeO_2 single crystals have allowed the symmetry of Raman modes to be unambiguously assigned. The nature of the vibrations has also been determined on the basis of the analysis of the eigendisplacement vectors of each Raman mode and the calculation of their localization entropy, contributing to clarify a long-standing debate in the literature. The localization entropy appears to be a relevant parameter to unambiguously assign Raman modes in α-quartz-type materials. It indicates in particular that Raman modes in α-GeO_2 are not very localized and that the main A_1 (TO3) line cannot be assigned to Ge−O−Ge bending, as recently reported by Kaindl et al.,[24] given the weak localization factor on Ge atoms (0.03), but actually corresponds to O−Ge−O twisting. The absence of any temperature-induced phase transition has been confirmed at the local level using variable temperature Raman spectroscopy measurements. From a vibrational and dynamic point of view, α-quartz GeO_2 is shown to be significantly different from α-quartz. In contrast to the latter, α-GeO_2 is found to exhibit very slightly anharmonic vibrations, as evidenced by the very low wavenumber shifts and the weak damping of the modes between room temperature and 1373 K. Furthermore, DFT calculations reveal that the A_1 mode (located at 264 cm^{-1}) involving only oxygen displacements is not a tetrahedral libration mode. This mode does not soften and broaden significantly with increasing temperature, even close to the melting point, indicating a low degree of thermally induced dynamic disorder.

AUTHOR INFORMATION

Corresponding Author

*E-mail: Guillaume.Fraysse@univ-lille1.fr (G.F.), pascale.armand@univ-montp2.fr (P.A.).

Present Address

[§]Unité Matériaux Et Transformations (UMET), CNRS UMR 8207, Université Lille 1. Bâtiment C6, 59655 Villeneuve d'Ascq, France.

Notes

The authors declare no competing financial interest.

ACKNOWLEDGMENTS

We would like to gratefully acknowledge Jérôme Debray (Institut Néel) for sample polishing, David Maurin and Dr. Jadna Catafesta for assistance with the polarized Raman experiment, and Dr. Thierry Michel (Laboratoire Charles Coulomb, Université Montpellier 2) for the use of the Jobin-Yvon T64000 Raman spectrometer.

REFERENCES

(1) Zhang, S.; Yu, F. *J. Am. Ceram. Soc.* **2011**, *94*, 3153−3170.
(2) Fritze, H. *J. Electroceram.* **2011**, *26*, 122−161.
(3) Damjanovic, D. *Curr. Opin. Solid State Mater. Sci.* **1998**, *3*, 469−473.
(4) Armand, P.; Beaurain, M.; Rufflé, B.; Menaert, B.; Papet, P. *Inorg. Chem.* **2009**, *48*, 4988−4996.
(5) Millichamp, J.; Ali, E.; Brandon, N. P.; Brown, R. J. C.; Hodgson, D.; Kalyvas, C.; Manos, G.; Brett, D. J. L. *Ind. Eng. Chem. Res.* **2011**, *50*, 8371−8375.
(6) Cambon, O.; Haines, J.; Fraysse, G.; Détaint, J.; Capelle, B.; Van der Lee, A. *J. Appl. Phys.* **2005**, *97*, 074110.
(7) Ranieri, V.; Darracq, S.; Cambon, M.; Haines, J.; Cambon, O.; Largeteau, A.; Demazeau, G. *Inorg. Chem.* **2011**, *50*, 4632−4639.
(8) Yu, F. P.; Zhao, X.; Pan, L. H.; Li, F.; Yuan, D. R.; Zhang, S. J. *J. Phys. D* **2010**, *43*, 165402.
(9) Zhang, S. J.; Frantz, E.; Xia, R.; Everson, W.; Randi, J.; Snyder, D. W.; Shrout, T. R. *J. Appl. Phys.* **2008**, *104*, 084103.
(10) Philippot, E.; Armand, P.; Yot, P.; Cambon, O.; Goiffon, A.; McIntyre, G. J.; Bordet, P. *J. Solid State Chem.* **1999**, *146*, 114−123.
(11) Haines, J.; Cambon, O.; Philippot, E.; Chapon, L.; Hull, S. *J. Solid State Chem.* **2002**, *166*, 434−442.
(12) Armand, P.; Clément, S.; Balitsky, D.; Lignie, A.; Papet, Ph. *J. Cryst. Growth* **2011**, *316*, 153−157.
(13) Lignie, A.; Armand, P.; Papet, P. *Inorg. Chem.* **2011**, *50*, 9311.
(14) Balitsky, D. V.; Balitsky, V. S.; Pisarevsky, Yu. V.; Philippot, E.; Silvestrova, O. Yu.; Pushcharovsky, D. Yu. *Ann. Chim. Sci. Mater.* **2001**, *26*, 183−192.
(15) Bhalerao, G. M.; Cambon, O.; Haines, J.; Levelut, C.; Mermet, A.; Sirotkin, S.; Menaert, B.; Debray, J.; Baraille, I.; Darrigan, C.; Rerat, M. *Inorg. Chem.* **2010**, *49*, 9470.
(16) Haines, J.; Cambon, O.; Keen, D. A.; Tucker, M. G.; Dove, M. T. *Appl. Phys. Lett.* **2002**, *81*, 1.
(17) Haines, J.; Cambon, O.; Prudhomme, N.; Fraysse, G.; Keen, D. A.; Chapon, L. C.; Tucker, M. G. *Phys. Rev. B* **2006**, *73*, 014103.
(18) Lucazeau, G. *J. Raman Spectrosc.* **2003**, *34*, 478−496.
(19) Lignie, A.; Granier, D.; Armand, P.; Haines, J.; Papet, P. *J. Appl. Crystallogr.* **2012**, *45*, 272−278.
(20) Damen, T. C.; Porto, S. P. S.; Tell, B. *Phys. Rev.* **1966**, *142*, 570.
(21) Gonze, X.; Amadon, B.; Anglade, P. M.; Beuken, J. M.; Bottin, F.; Boulanger, P.; Bruneval, F.; Caliste, D.; Caracas, R.; Cote, M.; Deutsch, T.; Genose, L.; Ghosez, Ph.; Giantomassi, M.; Goedecker, S.; Hamann, D.; Hermet, P.; Jollet, F.; Jomard, G.; Leroux, S.; Mancini, M.; Mazevet, S.; Oliveira, M. J. T.; Onida, G.; Pouillon, Y.; Rangel, T.; Rignanese, G.-M.; Sangalli, D.; Shaltaf, R.; Verstraete, M.; Zerah, G.; Zwanziger, J. W. *Comput. Phys. Commun.* **2009**, *180*, 2582.
(22) Perdew, J. P.; Wang, Y. *Phys. Rev. B* **1992**, *45*, 13244.
(23) Hermet, P.; Veithen, N.; Ghosez, Ph. *J. Phys.: Condens. Matter* **2007**, *19*, 456202.
(24) Kaindl, R.; Többens, D. M.; Penner, S.; Bielz, T.; Soisuwan, S.; Klötzer, B. *Phys. Chem. Miner.* **2012**, *39*, 47−55.
(25) Sendova-Vassileva, M.; Tzenov, N.; Dimova-Malinovskia, D.; Rosenbauer, M.; Stutzmann, M.; Josepovits, K. V. *Thin Solid Films* **1994**, *255*, 282−285.
(26) Mukherjee, S. P.; Sharma, S. K. *J. Am. Ceram. Soc.* **1986**, *11*, 806−810.
(27) Bielz, T.; Soisuwan, S.; Kaindl, R.; Tessadri, R.; Többens, D. M.; Klötzer, B.; Penner, S. *J. Phys. Chem. C* **2011**, *115*, 9706−9712.
(28) Scott, J. F. *Phys. Rev. B* **1970**, *1*, 3488−3493.
(29) Dultz, W.; Quilichini, M.; Scott, J. F.; Lehmann, G. *Phys. Rev. B* **1975**, *11*, 1648.
(30) Avakyants, L. P.; Gvozdkova, I. A.; Slobodyanyuk, A. V. *Opt. Spektrosk. (USSR)* **1990**, *69*, 952−955.
(31) Gillet, P.; Le Cléac'h, A.; Madon, M. *J. Geophys. Res.* **1990**, *95*, 635−655.
(32) Mernagh, T. P.; Liu, L. G. *Phys. Chem. Miner.* **1997**, *24*, 7−16.

(33) Ghobadi, E.; Capobianco, J. A. *Phys. Chem. Chem. Phys.* **2000**, *2*, 5761−5763.
(34) Micoulaut, M.; Cormier, L.; Henderson, G. S. *J. Phys.: Condens. Matter* **2006**, *18*, R753−R784.
(35) Atuchin, V. V.; Gavrilova, T. A.; Gromilov, S. A.; Kostrovsky, V. G.; Pokrovsky, L. D.; Troitskaia, I. B.; Vemuri, R. S.; Carbajal-Franco, G.; Ramana, C. V. *Cryst. Growth Des.* **2009**, *9*, 1829−1832.
(36) Ranieri, V.; Bourgogne, D.; Darracq, S.; Cambon, M.; Haines, J.; Cambon, O.; Leparc, R.; Levelut, C.; Largeteau, A.; Demazeau, G. *Phys. Rev. B* **2009**, *79*, 224304.
(37) Parke, S. Glasses. In *The infrared Spectra of Minerals*; Farmer, V. C., Ed.; Mineralogical Society, 1974; pp 483−514.
(38) Tucker, M. G.; Keen, D. A.; Dove, M. T. *Miner. Mag.* **2001**, *65*, 489.
(39) Gregora, I.; Magneron, N.; Simon, P.; Luspin, Y.; Raimboux, N.; Philippot, E. *J. Phys.: Condens. Matter* **2003**, *15*, 4487.
(40) McMillan, P. F.; Hess, A. C. *Phys. Chem. Miner.* **1990**, *17*, 97−107.
(41) Cambon, O.; Bhalerao, G. M.; Bourgogne, D.; Haines, J.; Hermet, P.; Keen, D. A.; Tucker, M. G. *J. Am. Chem. Soc.* **2011**, *133*, 8048−8056.